



1

2 **Physical pedotransfer functions to compute saturated hydraulic**
3 **conductivity from bimodal characteristic curves for a range of New**
4 **Zealand soils**

5 Joseph Aleander Paul Pollacco¹, Trevor Webb¹, Stephen McNeill¹, Wei Hu², Sam Carrick¹, Allan
6 Hewitt¹, Linda Lilburne¹

7 ¹ Landcare Research, PO Box 69040, Lincoln 7640, New Zealand

8 ² New Zealand Institute for Plant & Food Research Limited, Private Bag 4704, Christchurch 8140, New Zealand

9 *Correspondence to:* Joseph A.P. Pollacco (Pollacco.water@gmail.com)

10

11 **Abstract.** Descriptions of soil hydraulic properties, such as *soil moisture release curve*, $\theta(h)$, and *saturated hydraulic*
12 *conductivities*, K_s , are a prerequisite for hydrological models. Since the measurement of K_s is expensive, it is frequently
13 derived from pedotransfer functions. Because it is usually more difficult to describe K_s than $\theta(h)$ from pedotransfer
14 functions, Pollacco et al. (2013) developed a physical unimodal model to compute K_s solely from hydraulic parameters
15 derived from the Kosugi $\theta(h)$. This unimodal K_s model, which is based on a unimodal Kosugi soil pore-size distribution, was
16 developed by combining the approach of Hagen-Poiseuille with Darcy's law and by introducing three tortuosity parameters.
17 We report here on (1) the suitability of the Pollacco unimodal K_s model to predict K_s for a range of New Zealand soils, and
18 (2) further adaptations to this model to adapt it to dual-porosity structural soils by computing the soil water flux through a
19 continuous function of an improved bimodal pore-size distribution. The improved bimodal K_s model was tested with a New
20 Zealand data set derived from historical measurements of K_s and $\theta(h)$ for a range of soils derived from sandstone and
21 siltstone. The K_s data were collected using a small core size of 100 mm, causing large uncertainty in replicate measurements.
22 Predictions of K_s were further improved by distinguishing topsoils from subsoil. Nevertheless, as expected stratifying the
23 data with soil texture only slightly improved the predictions of the physical K_s models because the K_s model is based on
24 pore-size distribution and the calibrated parameters were obtained within the physically feasible range. The improvements
25 made to the unimodal K_s model by using the new bimodal K_s model are modest when compared to the unimodal model,
26 which is explained by the poor accuracy of measured total porosity. Nevertheless, the new bimodal model provides an
27 acceptable fit to the observed data. The study highlights the importance of improving K_s measurements with larger cores.

28

29

30 **Keywords.** saturated hydraulic conductivity; bimodal; pedotransfer functions; Kosugi model; soil moisture release curves;
31 Hagen-Poiseuille; tortuosity; soils; New Zealand; S-map

32

33 **Abbreviations.** **PTFs:** statistical pedotransfer functions; **PPTFs:** physically based pedotransfer functions; **S-map:** New
34 Zealand soil database; $\theta(h)$ soil moisture release curve; K_s saturated hydraulic conductivity

35



36 1 Introduction

37 Modelling of the water budget, irrigation, and nutrient and contaminant transport through the unsaturated zone requires
38 accurate soil moisture release, $\theta(h)$, and unsaturated hydraulic conductivity, $K(\theta)$, curves. The considerable time and cost
39 involved in measuring $\theta(h)$ and $K(\theta)$ directly for a range of soils mean that the information for specific soils of interest is
40 often not available (Webb, 2003). Therefore, these curves are generally retrieved from pedotransfer functions (PTFs), which
41 are statistical relationships that generate lower-precision estimates of physical properties of interest based on many rapid and
42 inexpensive measurements (e.g., Balland and Pollacco, 2008; Pollacco, 2008; Anderson and Bouma, 1973; Webb, 2003).

43

44 The S-map database (Lilburne et al., 2012; Landcare Research, 2015) provides soil maps for the most intensively used
45 land in New Zealand and is being gradually extended to give national coverage. S-map provides data for extensively used
46 soil models, such as the soil nutrient model OVERSEER and the daily simulation model APSIM used by agricultural
47 scientists. McNeill et al. (2012) used the New Zealand National Soils Database to derive PTFs to estimate $\theta(h)$ at five
48 tensions from morphological data of soils mapped in S-map. One of the current weaknesses of S-map is a lack of capacity to
49 estimate $K(\theta)$. Building on the work of Griffiths et al. (1999), Webb (2003) showed that morphologic descriptors for New
50 Zealand soils can be used to predict K_s . However, the predictions of K_s were found to be too coarse for application to the
51 wide range of soils within S-map. Therefore, Cichota et al. (2013) tested published statistical PTFs developed in Europe and
52 the USA to predict $\theta(h)$ and $K(\theta)$ for a range of New Zealand soils. They combined the best two or three PTFs to construct
53 ensemble PTFs. They considered the ensemble PTF for $\theta(h)$ to be a reasonable fit, but the ensemble PTF for estimating K_s
54 exhibited large scatter and was not as reliable. The poor performance when estimating K_s was possibly due to the absence of
55 any measurements of pore-size distribution in their physical predictors (Watt and Griffiths, 1988; McKenzie and Jacquier,
56 1997), and also to the large uncertainties in the measurements from small cores (McKenzie and Cresswell, 2002 ; Anderson
57 and Bouma, 1973). Consequently, there is an urgent need in New Zealand to develop a physically based pedotransfer
58 function (PPTF) model for K_s that is based on pore-size distribution.

59

60 Since PTFs developed to characterize $\theta(h)$ are more reliable than PTFs to characterize $K(\theta)$ (e.g., Balland and Pollacco,
61 2008; Cichota et al., 2013), Pollacco et al. (2013) developed a new class of physical pedotransfer function, PPTF, that
62 predicts unimodal K_s solely from hydraulic parameters derived from the Kosugi (1996) $\theta(h)$. The PPTFs are derived by
63 combining the Hagen-Poiseuille and Darcy law and by incorporating three semi-empirical tortuosity parameters. The model
64 is based on the soil pore-size distribution and has been successfully validated using the European HYPRES (Wösten et al.,
65 1998; Wösten et al., 1999; Lilly et al., 2008) and the UNSODA databases (Leij et al., 1999; Schaap and van Genuchten,
66 2006), but has not yet been applied to New Zealand soils. Most New Zealand soils are considered to be structural, with
67 two-stage drainage (Carrick et al., 2010; McLeod et al., 2008) and bimodal pore-size distribution (e.g. Durner, 1994).
68 Romano and Nasta (2016) showed by using the HYDRUS-1D package that large errors arise in the computation of the the
69 water fluxes if unimodal $\theta(h)$ and $K(\theta)$ are used in structural soils. We therefore propose to improve the unimodal Pollacco et
70 al. (2013) K_s PPTF model so that it can predict K_s for structural soils with bimodal porosity.

71

72 Measured K_s values exhibit notoriously high variability (Carrick, 2009). The variability is expected to increase as the
73 sampling diameter decreases because small cores provide an unrealistic representation of the abundance and connectivity of
74 macropores (McKenzie and Cresswell, 2002; Anderson and Bouma, 1973). McKenzie and Cresswell (2002) suggest that
75 laboratory measurements should use cores with minimum diameter and length of 10–30 cm, with 25 cm diameter and 20 cm
76 length the standard dimensions for Australian research. In New Zealand, K_s has been obtained by using small cores,



77 commonly with 10 cm diameter and 7.5 cm length. This has contributed to very high variability in measured K_s (Webb et al.,
 78 2000).

79 The objectives of this research were to:

- 80 • test the suitability of the unimodal Pollacco et al. (2013) K_s model to predict K_s from New Zealand soils
- 81 • develop a K_s bimodal model that makes predictions in structural soils solely from hydraulic parameters derived
 82 from the Kosugi $\theta(h)$
- 83 • derive the uncertainties of the predictions of the K_s bimodal model
- 84 • provide recommendations on the critical data sets that are required to improve the S-map database in New Zealand.

85 2 Background

86 2.1 Kosugi unimodal characteristic and unsaturated hydraulic conductivity curve

87 There are a number of closed-form unimodal expressions in the literature that compute the soil moisture release curve $\theta(h)$
 88 and the unsaturated hydraulic conductivity $K(\theta)$ curves, such as the commonly used van Genuchten (1980) and Brooks and
 89 Corey (1964) curves. We selected the physically based Kosugi (1996) closed-form unimodal log-normal function expression
 90 of $\theta(h)$ and $K(\theta)$ because its parameters are theoretically sound and relate to the soil pore-size distribution (Hayashi et al.,
 91 2009). Soils have a large variation in pore radius, r , which follows a log-normal probability density function. The unimodal
 92 Kosugi log-normal probability density function of pore radius (r) is often written in the following form:

$$93 \quad \frac{d\theta}{dr} = \frac{\theta_s - \theta_r}{r\sigma\sqrt{2\pi}} \exp\left\{-\frac{[\ln(r/r_m)]^2}{2\sigma^2}\right\} \quad (1)$$

94 where θ_r and θ_s [$\text{cm}^3 \text{cm}^{-3}$] are the *residual* and *saturated water contents*, respectively; $\ln(r_m)$ [cm] and σ [-] are the mean and
 95 variance of the log-transformed soil-pore radius, $\ln(r)$, respectively.

96 Let S_e denote the effective saturation, defining $S_e(r) = (\theta - \theta_r)/(\theta_s - \theta_r)$, such that $0 \leq S_e \leq 1$. Integrating Eq. (1)
 98 from 0 to r yields the unimodal *characteristic curve* as a function of r :

$$99 \quad S_e(r) = \frac{1}{2} \operatorname{erfc}\left[\frac{\ln r_m - \ln r}{\sigma\sqrt{2}}\right] \quad (2a)$$

$$100 \quad \text{with } r = \frac{r_m}{\exp\left[\operatorname{erfc}^{-1}[2S_e]\sigma\sqrt{2}\right]} \quad (2b)$$

101 where erfc is the complementary error function.

102
 103 The Young–Laplace capillary equation relates the soil-pore radius, r , to the equivalent *matric suction head*, h (cm), at
 104 which the pore is filled or drained (i.e., $r = Y/h$, where $Y = 0.149 \text{ cm}^2$). Kosugi's unimodal *moisture release curve* $\theta_{\text{uni}}(h)$ can
 105 be written in terms of S_e :

$$106 \quad S_e(h) = \frac{1}{2} \operatorname{erfc}\left[\frac{\ln h - \ln h_m}{\sigma\sqrt{2}}\right] \quad (3)$$

107 where $\ln(h_m)$ and σ represent the mean and standard deviation of $\ln(h)$, respectively.

108



109 The unimodal Kosugi unsaturated hydraulic conductivity function $K(\theta)$ is written as:

$$110 \quad K(S_e) = K_s \sqrt{S_e} \left\{ \frac{1}{2} \operatorname{erfc} \left[\operatorname{erfc}^{-1}(2S_e) + \frac{\sigma}{\sqrt{2}} \right] \right\}^2 \quad (4)$$

111 where K_s (cm day⁻¹) is the saturated hydraulic conductivity.

112

113 θ_s is computed from the total porosity, ϕ , which is deduced from *bulk density* (ρ_b) and *soil particle density* (ρ_p) as follows:

$$114 \quad \phi = \left[1 - \frac{\rho_b}{\rho_p} \right] \quad (5)$$

115 Due to air entrapment, θ_s seldom reaches saturation of the total pore space ϕ (Carrick et al., 2011). Therefore, to take into

116 account the fact that not all pores are connected, we perform the following correction of ϕ with α in the range [0.9, 1]:

$$117 \quad \theta_s = \alpha \phi \quad (6)$$

118 It is accepted that $\alpha = 0.95$ (Rogowski, 1971; Pollacco et al., 2013; Haverkamp et al., 2005; Leij et al., 2005), but in this

119 study the optimal α was found to be 0.98, since using a value of 0.95 resulted in several soil samples with θ_s (θ measured

120 at 5 kPa) greater than θ_s , which is not physically plausible. This was due to the inaccuracy of measuring ϕ (discussed in

121 Sect. 4.1.2).

122 The feasible range of the Kosugi hydraulic parameters is summarized in Table 1. The h_m and σ feasible range is taken

123 from Pollacco et al. (2013), who combined data from the HYPRES (Wösten et al., 1998; Wösten et al., 1999; Lilly et al.,

124 2008) and UNSODA (Leij et al., 1999; Schaap and van Genuchten, 2006) databases.

125

126 **Table 1. please insert here**

127 2.2 Pollacco unimodal saturated hydraulic conductivity model

128 The *saturated hydraulic conductivity* model, K_{s_uni} (Pollacco et al., 2013) computes K_s from the Kosugi parameters θ_s , θ_r , σ

129 and h_m (or r_m). K_{s_uni} is based on the pore-size distribution (Eq. (1)) and the tortuosity of the pores. K_{s_uni} was derived by

130 adopting the method of Childs and Collisgeorge (1950) and modelling the soil water flux through a continuous function of

131 Kosugi (1996) pore-size distribution. This was performed by combining the Hagen-Poiseuille equation with Darcy's law and

132 introducing the connectivity and tortuosity parameters τ_1 , τ_2 of Fatt and Dykstra (1951) and τ_3 of Vervoort and Cattle (2003).

133 K_{s_uni} is computed as:

$$134 \quad K_{s_uni}(S_e) = C (1 - \tau_1) (\theta_s - \theta_r)^{\frac{1}{1-\tau_3}} \int_0^{S_e} r^{2(1-\tau_2)} dS_e \quad (7)$$

$$135 \quad \text{with } C = \frac{1}{8} \frac{\rho_w g}{\eta}$$

136 where for water at 20°C, density of water $\rho_w = 0.998$ g cm⁻³, acceleration due to gravity $g = 980.66$ cm s⁻², dynamic viscosity

137 of water $\eta = 0.0102$ g cm⁻¹ s⁻¹ and C is a constant equal to 1.03663×10^9 cm day⁻¹.

138

139 Integrating with S_e instead of r avoids the complication of finding the minimum and maximum value of r . Isolating r of

140 Eq. (2b) and replacing it in Eq. (7) gives:



$$141 \quad K_{s_uni}(S_e) = C (1 - \tau_1) (\theta_s - \theta_r)^{\frac{1}{1-\tau_3}} \int_0^{S_e} \left\{ \frac{Y/h_m}{\exp \left[\operatorname{erfc}^{-1}(2 S_e) \sigma \sqrt{2} \right]} \right\}^{2(1-\tau_2)} dS_e \quad (8a)$$

$$142 \quad \text{or } K_{s_uni}(S_e) = C (1 - \tau_1) (\theta_s - \theta_r)^{\frac{1}{1-\tau_3}} \int_0^{S_e} \left\{ \frac{r_m}{\exp \left[\operatorname{erfc}^{-1}(2 S_e) \sigma \sqrt{2} \right]} \right\}^{2(1-\tau_2)} dS_e \quad (8b)$$

143 and $r_m = Y/h_m$

144 where τ_1, τ_2, τ_3 are tortuosity parameters [0–1].

145

146 Note that $K_s = K_{s_uni}(S_e = 1)$ (Eq. (8)). If tortuosity were not included ($\tau_1, \tau_2, \tau_3 = 0$), the pore-size distribution model
 147 would mimic the permeability of a bundle of straight capillary tubes. Vervoort and Cattle (2003) state: “In reality soils are
 148 much more complex, with twisted and crooked pores, dead-ending or connecting to other pores. This means that there is a
 149 need to scale the permeability from the capillary tube model to include increased path length due to crookedness of the path
 150 (tortuosity) or lack of connection between points in the soil (connectivity)”. Soils that are poorly connected and have highly
 151 crooked pathways theoretically have $\tau_1, \tau_2, \tau_3 \approx 0.9$. Further explanation of tortuosity is provided in Table 2.

152

153

Table 2. Please insert here

154 2.3. Romano bimodal characteristic curve

155 New Zealand soils are predominantly well structured, with two-stage drainage (Carrick et al., 2010; McLeod et al., 2008),
 156 and therefore have a bimodal pore-size distribution (e.g. Durner, 1994). As K_{s_uni} is based on a unimodal curve, $\theta_{uni}(h)$, the
 157 proposed bimodal model, K_{s_bim} , should be based on a bimodal $\theta_{bim}(h)$ curve.

158

159 Borgesen et al. (2006) showed that structured soils have both *matrix* (inter-aggregate) pore spaces and *macropore*
 160 (intra-aggregate) pore spaces. Thus, when the pores are initially saturated ($r > R_{mac}$) or ($h < H_{mac}$), the flow is considered
 161 *macropore* flow, and when the soil is desaturated ($r < R_{mac}$) or ($h > H_{mac}$), the flow is considered *matrix* flow, as shown in
 162 Fig. 1. R_{mac} is the theoretical pore size r that delimits macropore and matrix flow. To model bimodal pore-size distribution
 163 Durner (1994) superposes two unimodal pore-size distributions by using an empirical weighting factor, W , which partitions
 164 the volumetric percentage of macropore and matrix pores. Recently Romano et al. (2011) proposed the following Kosugi
 165 bimodal $\theta_{bim_rom}(h)$ distribution:

$$166 \quad \theta_{bim_rom}(h) = (\theta_s - \theta_r) \left\{ W \operatorname{erfc} \left[\frac{\ln h - \ln h_{m_mac}}{\sigma_{mac} \sqrt{2}} \right] + (1 - W) \operatorname{erfc} \left[\frac{\ln h - \ln h_m}{\sigma \sqrt{2}} \right] \right\} + \theta_r \quad (9)$$

167 where $\theta_s, \ln(h_{m_mac})$ and σ_{mac} are, respectively, the *saturated water content*, the *mean* and the *standard deviation* of $\ln(h)$ of
 168 the macropore domain, θ_r, h_m and σ are parameters of the matrix domain, and W is a constant in the range [0,1].



169 3 Theoretical development of novel bimodal saturated hydraulic conductivity

170 We report on further adaptations to the physical model of Pollacco et al. (2013) to suit it to dual-porosity structural soils,
 171 which are common in New Zealand, solely from Kosugi hydraulic parameters describing $\theta(h)$. This involves:

- 172 • rewriting the Romano bimodal $\theta(h)$ (Sec. 3.1),
- 173 • developing a novel bimodal K_s model based on the modified bimodal $\theta(h)$ (Sec. 3.2).

174 3.1 Modified Romano bimodal characteristic curve

175 We propose a modified version of $\theta_{\text{bim_roml}}(h)$ (Eq. (9)) that does not use the empirical parameter W . Our modified function,
 176 $\theta_{\text{bim}}(h)$, is plotted in Fig. 1 and is computed as:

$$178 \quad \theta_{\text{bim}}(h) = \theta_{\text{bim_mac}}(h) + \theta_{\text{bim_mat}}(h) \quad (10a)$$

$$179 \quad \theta_{\text{bim_mac}}(h) = [\theta_s - \theta_{s_mac}] \operatorname{erfc} \left[\frac{\ln h - \ln h_{m_mac}}{\sigma_{mac} \sqrt{2}} \right] \quad (10b)$$

$$180 \quad \theta_{\text{bim_mat}}(h) = [\theta_{s_mac} - \theta_r] \operatorname{erfc} \left[\frac{\ln h - \ln h_m}{\sigma \sqrt{2}} \right] + \theta_r \quad (10c)$$

181 where θ_{s_mac} is the *saturated water content* that theoretically differentiates *macropore* and *matrix* domains.

182
 183 The shape of $\theta_{\text{bim}}(h)$ is identical to that of $\theta_{\text{bim_roml}}(h)$, but the advantage of $\theta_{\text{bim}}(h)$ is that it uses the physical parameter
 184 θ_{s_mac} instead of the empirical parameter W , and θ_{s_mac} is more easily parameterized than W . θ_{s_mac} is determined by fitting the
 185 hydraulic parameters θ_{s_mac} , θ_r , h_m , σ of $\theta_{\text{bim_mat}}(h)$ (Eq. (10c)) solely in the matrix range ($r < R_{\text{mac}}$ or $h > H_{\text{mac}}$) by ensuring
 186 that $\theta_{s_mac} < \theta_s$. Fig. 1 shows that R_{mac} and θ_{s_mac} delimit the matrix and the macropore domains and that r_m of the Kosugi
 187 model is the inflection point of $\theta_{\text{bim_mat}}(h)$ and r_{m_mac} is the inflection point of $\theta_{\text{bim_mac}}(h)$.

188
 189 **Fig. 1. Please put it here**

190 3.2 Novel bimodal saturated hydraulic conductivity model

191 Using $\theta_{\text{bim}}(h)$, we propose a new bimodal $K_{s_bim}(S_e)$ that is derived following $K_{s_uni}(S_e)$ (Eq. (7)) but for which we add a
 192 macropore domain:

$$193 \quad K_{s_bim}(S_e) = K_{s_bim_mat}(S_e) + K_{s_bim_mac}(S_e) \quad (11a)$$

$$194 \quad K_{s_bim_mat}(S_e) = C \int_0^{S_e} \left[(1 - \tau_1) (\theta_{s_mac} - \theta_r)^{\frac{1}{1-\tau_3}} r_{\text{matrix}}^{2(1-\tau_2)} \right] dS_e \quad (11b)$$

$$195 \quad K_{s_bim_mac}(S_e) = C \int_0^{S_e} \left[(1 - \tau_{1_mac}) (\theta_s - \theta_{s_mac})^{\frac{1}{1-\tau_{3_mac}}} r_{\text{macropore}}^{2(1-\tau_{2_mac})} \right] dS_e \quad (11c)$$

196 where $r_{\text{macropore}}$ is $r \geq R_{\text{mac}}$ and r_{matrix} is $r < R_{\text{mac}}$.

197 The r_{matrix} of Eq. (11b) is derived from Eq. (2b):

$$198 \quad r_{\text{matrix}} = \frac{r_m}{\exp \left[\operatorname{erfc}^{-1} [2 S_e] \sigma \sqrt{2} \right]} \quad (12)$$



199 and $r_{\text{macropore}}$ is computed similarly as:

$$200 \quad r_{\text{macropore}} = \frac{r_{m_mac}}{\exp \left[\operatorname{erfc}^{-1} [2 S_e] \sigma_{_mac} \sqrt{2} \right]} \quad (13)$$

201

202 We introduced r_{matrix} (Eq. (12)) and $r_{\text{macropore}}$ (Eq. (13)) into K_{s_bim} (Eq. (11a)), giving the equation for K_{s_bim} :

$$203 \quad K_{s_bim}(S_e) = C \int_0^{S_e} \left[\begin{aligned} & (1 - \tau_{1_mac}) (\theta_s - \theta_{s_mac})^{\frac{1}{1-\tau_{3_mac}}} \left\{ \frac{r_{m_mac}}{\exp \left[\operatorname{erfc}^{-1} [2 S_e] \sigma_{_mac} \sqrt{2} \right]} \right\}^{2(1-\tau_{2_mac})} + \\ & (1 - \tau_1) (\theta_{s_mac} - \theta_r)^{\frac{1}{1-\tau_3}} \left\{ \frac{r_m}{\exp \left[\operatorname{erfc}^{-1} [2 S_e] \sigma \sqrt{2} \right]} \right\}^{2(1-\tau_2)} \end{aligned} \right] dS_e \quad (14a)$$

204 or

$$205 \quad K_{s_bim}(S_e) = C \int_0^{S_e} \left[\begin{aligned} & (1 - \tau_{1_mac}) (\theta_s - \theta_{s_mac})^{\frac{1}{1-\tau_{3_mac}}} \left\{ \frac{\frac{Y}{h_{m_mac}}}{\exp \left[\operatorname{erfc}^{-1} (2 S_e) \sigma_{_mac} \sqrt{2} \right]} \right\}^{2(1-\tau_{2_mac})} + \\ & (1 - \tau_1) (\theta_{s_mac} - \theta_r)^{\frac{1}{1-\tau_3}} \left\{ \frac{\frac{Y}{h_m}}{\exp \left[\operatorname{erfc}^{-1} (2 S_e) \sigma \sqrt{2} \right]} \right\}^{2(1-\tau_2)} \end{aligned} \right] dS_e \quad (14b)$$

206

207 In Eq. (14b), r_{m_mac} is replaced by Y/h_{m_mac} and r_m is replaced by Y/h_m and for the computation of K_s than $K_{s_bim}(S_e = 1)$. Note
 208 that the bimodal K_s model requires that the flow in the macropore domain obeys the Buckingham–Darcy law. Therefore, this
 209 model's performance may be restricted in cases of non-Darcy flow, such as non-laminar and turbulent flow, which may
 210 occur in large macropores.

211

212 In this study $\sigma_{_mac}$ is not derived from measured $\theta(h)$ because measured data in the macropore domain are difficult to
 213 find, and so it will be treated as a fitting parameter. As discussed above, θ_{s_mac} , θ_r , σ and h_m are optimized with $\theta_{\text{un}}(h)$
 214 measurement points only in the matrix range ($r < R_{\text{mac}}$ or $h > H_{\text{mac}}$), which means that θ_s is not included in the observation
 215 data. In summary, K_{s_bim} requires optimization of the parameters τ_1 , τ_2 , τ_3 , and τ_{1_mac} , τ_{2_mac} , τ_{3_mac} and h_{m_mac} , $\sigma_{_mac}$ (if no
 216 data are available in the macropore domain). The theoretically feasible range of the parameters of K_{s_bim} is shown in Table 3.

217

Table 3. Please put table here.

218

219 One of the limitations of the New Zealand data set is that it has no $\theta(h)$ data points in the macropore domain. The
 220 closest data point near saturation is $\theta(h = 50 \text{ cm})$, which is in the matrix pore space. Carrick et al. (2010) found that H_{mac}
 221 ranges from 5 to 15 cm, with an average $H_{\text{mac}} = 10 \text{ cm}$, which corresponds to a circular pore radius of $R_{\text{mac}} = 0.0149 \text{ cm}$ (e.g.
 222 Jarvis, 2007; Jarvis and Messing, 1995; Messing and Jarvis, 1993). Therefore, to reduce the number of optimized parameters
 223 we make the following assumption:



$$h_{m_mac} = \exp \left[\frac{\ln(H_{mac})}{2} \right] \quad (15)$$

225 To illustrate this, the equivalent r_{m_mac} (h_{m_mac}) point is shown in Fig. 1, where r_{m_mac} is the inflection point of the macropore
 226 domain. The value 2 was found to be optimal. Fig. 1 also shows that the matrix and the macropore domains meet at R_{mac}
 227 (H_{mac}).

228 4 Methods

229 4.1 Data

230 4.1.1 Selecting soil samples from New Zealand Soils Database

231 The soils data used in this study were sourced from two data sets. The first data set (Canterbury Regional Study; Table
 232 4) soils were derived from eight soils series on the post-glacial and glacial surfaces of the Canterbury Plains (Webb et al.,
 233 2000). The soils varied from shallow, well-drained silt loam soils to deep, poorly drained clay loam soils. Each soil series
 234 had nine profiles. Three horizons in each soil profile were sampled from deep soils (topsoil, horizon with slowest
 235 permeability, and the main horizon between these) and two from shallow soils (topsoil and the main horizon above gravels).
 236 Grab samples were taken for particle size analysis, a 5.5 cm diameter core was taken from the middle of each horizon for
 237 moisture release analysis, and three 10 cm diameter cores were taken from the upper part of each horizon for hydraulic
 238 conductivity analysis.

239 The second data set was derived from the Soil Water Assessment and Measurement Programme to physically
 240 characterize key soils throughout New Zealand in the 1980s. Soils selected from this data set are listed by region in Table 4.
 241 All soils selected were from soils formed from sediments derived from indurated sandstone rocks, because this is the most
 242 common parent material for soils in New Zealand and has a reasonably representative number of soils analysed for physical
 243 properties. Selection of horizons and core size was similar to the Canterbury regional study, except that more subsoil
 244 horizons were sampled at some sites, cores for hydraulic conductivity were not sampled in the topsoil horizon, and four to
 245 six cores for hydraulic conductivity were sampled in subsoils.

246 4.1.2 Measuring characteristic curves and total porosity

247 Laboratory analysis for particle size followed Gradwell (1972). The soil moisture release curves were derived by using 55
 248 mm diameter cores according to the methods of Gradwell (1972).

249
 250 The total porosity, ϕ , described in Eq. (5) contains uncertainties from the measurement methods, where ϕ is derived
 251 from separate measurements of particle density and bulk density, rather than being directly measured. The uncertainty in ϕ
 252 measurements appeared to have reduced the demonstrated benefits of using K_{s_bim} instead of K_{s_uni} , which strongly relies on
 253 $\phi \alpha - \theta_{s_mac}$ and may have caused the optimal α to be 0.98 and not the commonly accepted value of 0.95 (Rogowski, 1971;
 254 Pollacco et al., 2013; Haverkamp et al., 2005; Leij et al., 2005).

255

256

Table 4. Please put here

257 4.1.3 Measuring saturated hydraulic conductivity performed with problematic small cores

258 The K_s data used were collected and processed at a time when the best field practices in New Zealand were still being
 259 explored. K_s was derived using constant-head Mariotte devices (10 mm head) from three to six cores (100 mm diameter and



260 7.5 cm thickness) for each horizon. The \log_{10} scale value of the standard error of the replicates of the measurements is shown
 261 in Fig. 2, which shows large uncertainty in the measurements (up to three orders of magnitude). This uncertainty is due to:

- 262 a) **measurements of $\theta(h)$ and K_s being taken on different cores**, which caused some mismatch between $\theta(h)$ and K_s ,
 263 resulting in 16 outliers that negatively influenced the overall fit of the K_s model having to be removed from the data set
- 264 b) **side leakage** of some cores, which led to K_s values that were too high (Carrick, 2009), resulting in six samples with
 265 unusually high K_s having to be removed from the data set
- 266 c) **misreporting low K_s** since the measurements of K_s were halted when conductivity was less than 0.1 cm day^{-1} , resulting
 267 in four samples with low K_s having to be removed from the data set
- 268 d) **small core samples**, which led to considerable variability in the absence/presence of structural cracks caused by roots
 269 or worm burrows (McKenzie and Cresswell, 2002; Anderson and Bouma, 1973) that were evident in dyed samples; we
 270 therefore removed measured K_s replicates that were too high and showed evidence of macropore abundance by having
 271 values of $\theta_s - \theta_{s_mac} > 0.05$.

272 We therefore selected 235/262 samples (90%) and removed only 27 outliers, which is minimal compared, for instance, to the
 273 UNSODA (Leij et al., 1999; Schaap and van Genuchten, 2006) and HYPRES databases (Wösten et al., 1998; Wösten et al.,
 274 1999; Lilly et al., 2008), which are used for the development of PTFs such as the ROSETTA PTF (Patil and Rajput, 2009;
 275 Rubio, 2008; Young, 2009), and which were found to contain a large number of outliers. Using these databases, Pollacco et
 276 al. (2013) selected only 73/318 soils (23%), which complied with strict selection criteria prior to modelling.

277

278 Note that the K_s observations in the topsoils have greater variability than in the subsoil layers (Fig. 2). This is because
 279 topsoils are more disturbed by tillage, planar fissures formed by wetting/drying, compaction, growth of plant roots and
 280 earthworm burrowing. Therefore, the topsoils also have a greater abundance of macropores, and therefore are more prone to
 281 error when the sampling is performed with a small core size that does not contain a representative volume of the macropore
 282 network.

283

284

Fig. 2. Please insert figure here

285 4.2 Inverse modelling

286 The parameterization of the model was performed in two consecutive steps:

- 287 1. Optimization of θ_{s_mac} , θ_r , h_m and σ of the unimodal Kosugi $\theta_{bim_mat}(h)$ (Eq. (10c)) was performed by matching
 288 observed and simulated $\theta(h)$ in the range $h < H_{mac}$ (as discussed, θ_s is not included in the observation data). The
 289 feasible ranges of the Kosugi parameters are described in Table 1.
- 290 2. Optimization of the τ_1 , τ_2 , τ_3 of the K_{s_uni} model (Eq. (8)) and τ_{1_mac} , τ_{2_mac} , τ_{3_mac} , σ_{mac} parameters of the K_{s_bim}
 291 models (Eq. (14)), where the physical feasible ranges of the tortuosity parameters are described in Table 3.

292 The inverse modelling was performed using AMALGAM in MATLAB, which is a robust global optimization algorithm
 293 (<http://faculty.sites.uci.edu/jasper/sample/>) (e.g., ter Braak and Vrugt, 2008). For each step we minimized the objective
 294 functions described below.

295 4.2.1 Inverting the Kosugi hydraulic parameters

296 The objective function, OF_{θ} , used to parameterize Kosugi's $\theta(h)$ at the following pressure points [5, 10, 20, 40, 50, 100,
 297 1500 kPa], is described by:



$$298 \quad OF_{\theta} = \sum_{i=1}^{i=N_{\theta}} [\theta_{sim}(h_i, \mathbf{p}_{\theta}) - \theta_{obs}(h_i)]^{P_{over}} \quad (16)$$

299 where the subscripts *sim* and *obs* are simulated and observed, respectively. \mathbf{P}_{θ} is the set of predicted parameters (θ_{s_mac} , h_m , σ)
 300 and P_{over} is the power of the objective function.

301 The computation of K_{s_bim} requires $\theta(h)$ to be accurate near saturation, when the drainage is mostly from large pores,
 302 and to achieve this we make P_{over} large (equal to 6).

303 4.2.2 Calibrating the tortuosity parameters of the saturated hydraulic conductivity model

304 The parameters of K_{s_uni} and K_{s_bim} models were optimized by minimizing the following objective function OF_{ks} :

$$305 \quad OF_{ks} = \sum_{j=1}^{j=N_{ks}} [\ln K_{s_sim}(\mathbf{p}_{ks}) - \ln K_{s_obs}]^2 \quad (17)$$

306 where the subscripts *sim* and *obs* are simulated and observed, respectively. \mathbf{P}_{ks} is the vector of the unknown parameters. The
 307 log transformation of OF_{ks} puts more emphasis on the lower $K(\theta)$ and therefore reduces the bias towards larger conductivity
 308 (e.g. van Genuchten et al., 1991; Pollacco et al., 2011). Also, the log transformation considers that the uncertainty in
 309 measured unsaturated hydraulic conductivity increases as $K(\theta)$ increases.

310
 311 The following transformation was necessary to scale the parameters to enable the global optimization to converge to a
 312 solution:

$$313 \quad \tau_1 = 1 - 10^{-T_1} \quad (18)$$

314 where T_1 is a transformed tortuosity τ_1 .

315

316 Introducing Eq. (18) into K_{s_bim} Eq. (14) gives:

$$317 \quad K_{s_bim}(S_e) = C \int_0^{S_e} \left[\begin{array}{l} 10^{-T_{1_mac}} (\theta_s - \theta_{s_mac})^{\frac{1}{1-\tau_3_mac}} \left\{ \frac{\frac{Y}{h_{m_mac}}}{\exp \left[\operatorname{erfc}^{-1}(2 S_e) \sigma_{mac} \sqrt{2} \right]} \right\}^{2(1-\tau_2_mac)} + \\ 10^{-T_1} (\theta_{s_mac} - \theta_r)^{\frac{1}{1-\tau_3}} \left\{ \frac{\frac{Y}{h_m}}{\exp \left[\operatorname{erfc}^{-1}(2 S_e) \sigma \sqrt{2} \right]} \right\}^{2(1-\tau_2)} \end{array} \right] dS_e \quad (19)$$

318 5 Results and discussion

319 We report on (1) the suitability of the K_{s_uni} model (European and American data sets, Pollacco et al., 2013) to predict K_s for
 320 New Zealand soils experiencing large uncertainties, as shown in Fig. 2; (2) improvements made by stratifying the data with
 321 texture and topsoil/subsoil; and (3) improvements made by using the bimodal K_{s_bim} instead of the unimodal K_{s_uni} . The
 322 goodness of fit between simulated (K_{s_uni} or K_{s_bim}) and observed K_s was computed by the RMSElog₁₀:



$$RMSE_{\log_{10}} = \sqrt{\frac{\sum_{j=1}^{j=N_{K_s}} [\log_{10} K_{s_sim} - \log_{10} K_{s_obs}]^2}{N}} \quad (20)$$

where N is the number of data points.

5.1 Improvement made by stratifying with texture and topsoil/subsoil

It was expected that stratifying with texture and topsoil/subsoil (layers) should improve the predictions of K_s to only a modest degree. This is because K_{s_bim} and K_{s_uni} are physically based models that are based on pore-size distribution, and therefore stratifying with soil texture or topsoil/subsoil are not likely to provide extra information. For instance, Arya and Paris (1981) showed that there is a strong relationship between pore-size distribution and the particle-size distribution and therefore adding soil texture information should not improve the model.

Table 5. please put table here

As expected, no significant improvements were made by stratifying with soil texture compared with a model that groups all texture classes (loam and clay) and layers (topsoil and subsoil) (overall improvement of 3%) (Table 5). However, a significant improvement was made by stratifying by layer (topsoil and subsoil) (overall improvement of 23%), and therefore the remaining results are presented by stratifying by layer. These results are obtained because topsoils have higher macropores and a smaller tortuous path than that in subsoil, as demonstrated by $\tau_{1_top} > \tau_{1_sub}$ or $T_{1_top} < T_{1_sub}$, $\tau_{2_top} > \tau_{2_sub}$, $\tau_{3_top} > \tau_{3_sub}$ (Table 6). It is important to note that tortuosity decreases as τ becomes closer to 1.

Table 6. Please put table here

5.2 Improvement made by using K_{s_bim} instead of K_{s_uni}

Figure 3 shows an acceptable fit between K_{s_bim} and K_{s_obs} ($RMSE_{\log_{10}} = 0.450 \text{ cm day}^{-1}$), recognizing that the observations contain large uncertainties since the measurements were taken by using small cores (Sect. 4.1.3). The overall improvement made by using K_{s_bim} is somewhat modest (5% for all soils). As expected, the improvement is greater for topsoil containing higher macroporosity (12% improvement) than for subsoil (4% improvement) (Table 6). This is because topsoil has higher macropore θ_{mac} ($\theta_s - \theta_{s_mac}$) (Table 7) caused by earthworm channels, fissures, roots and tillage than subsoil.

Table 7. Please put table here

The reason K_{s_bim} shows smaller-than-expected improvements compared to K_{s_uni} requires further investigation and testing with a data set containing fewer uncertainties. One plausible explanation is that K_{s_bim} is highly sensitive to θ_s , computed from total porosity ϕ (Eq. (6)), which had inherent measurement uncertainties (Sect. 4.1.2). In addition, the possible existence of non-Darcy flow in large biological pores may decrease the outperformance of the bimodal model over the unimodal model.

Fig. 3. Please insert Figure 3 here

5.2 Optimal tortuosity parameters

The optimal tortuosity parameters of K_{s_bim} and K_{s_uni} (Table 6) show that the optimal parameters are within the physically feasible limits, except for τ_{3_mac} of the subsoil, which are greater than τ_3 . This is understandable because Pollacco et al. (2013) found τ_3 not to be a very sensitive parameter. As expected, T_{1_mac} is smaller than T_1 ($\tau_{1_mac} > \tau_1$), which suggests that the tortuosity parameters have a physical meaning.



358

359 The estimated value of the unimodal T_1 parameter K_{s_uni} derived from the UNSODA and HYPRES data sets ($T_1 = 0.1$)
 360 (Pollacco et al., 2013) is very different from the value estimated in this present study ($T_1 = 6.5$). Cichota et al. (2013) also
 361 reported that PTFs developed in Europe and the USA were not applicable to New Zealand. The reasons why these PTFs are
 362 not directly applicable to New Zealand require further investigation.

363 5.3 Uncertainty of the bimodal saturated hydraulic conductivity model predictions

364 The practical application of the bimodal saturated hydraulic conductivity model, K_{s_bim} , to New Zealand soils requires a
 365 model for the uncertainty of the resultant predictions, since it is then possible to attach a value for the uncertainty of future
 366 predictions of K_s . In a conventional parametric statistical model, the uncertainty model follows from the structure of the
 367 fitting model itself. In the present work, K_s is estimated using an inverse model and this has no associated functional
 368 uncertainty model. For this reason, the uncertainty is derived empirically by fitting a relationship between the transformed
 369 residuals of the model (the log-transformed measured K_s minus the log-transformed estimated K_s) as a function of the
 370 log-transformed estimated K_s . Although the uncertainty model could be derived from all the soils in the study, this results in
 371 a pooled estimate for uncertainty (e.g., aggregated root mean square error). However, it has been observed that topsoils and
 372 subsoils have different uncertainty behaviour for the estimated K_s , so it is desirable to include an indicator variable to
 373 determine whether the soil is a topsoil or not. In explicit form,

$$374 \quad \log_{10} K_{s\ obs} - \log_{10} K_{s\ sim} = a_1 L + a_0 + \epsilon \quad (21)$$

375 where a_0 and a_1 are fitting constants, L is an indicator variable specifying whether the soil is a topsoil (value 1), or a
 376 subsoil (value 0), and ϵ is the uncertainty distribution. The distribution of the uncertainty ϵ could take a number of forms,
 377 but there is no obvious choice, except that one might expect the distribution central measure to be unbiased. To avoid an
 378 explicit distribution assumption, we fitted a conditional quantile model (Koenker, 2005) for the transformed residuals, based
 379 on the τ quantile, where $\tau = 0.5$ corresponds to the conditional median, and $\tau = 0.025$ and $\tau = 0.975$ correspond
 380 respectively to the 2.5% and 97.5% quantiles, and thus describe the 95% containment interval of the residuals.

381 The conditional quantile model Eq. (21) was fitted using $\tau = 0.5, 0.025$ and 0.975 (Table 8). The results suggest a
 382 strong dependence of the scale of the residuals on whether the soil is a topsoil or not, but the size of the 95% residual
 383 containment interval is not dependent on the simulated K_s . Notably, the confidence interval for the fitted median ($\tau = 0.5$)
 384 quantile model suggests that the uncertainty distribution median is unbiased; thus predictions from K_{s_bim} show no propensity
 385 for bias, which is a desirable result.

386

Table 8. Please put here

387 Another way to illustrate the uncertainty model is to plot the observed $\log_{10} K_{s\ obs}$ against the estimated $\log K_{s\ bim}$,
 388 with the fitted median, lower and upper 95% quantile lines, as shown in Fig. 4. The width of the 95% containment interval
 389 for the residuals is narrower (i.e., the predictions appear to be more accurate) for topsoils. The quantile estimates for the
 390 conditional median of both topsoil and subsoil are also shown in Fig. 4, with the shaded region showing the 95% confidence
 391 interval of the median estimate. The shaded region covers the one-to-one line in Fig. 4, and thus there is no compelling
 392 evidence that the median residual distribution is biased.

393

Fig. 4. Please put here



394 5.4 Recommended future work to improve the New Zealand soil database

395 A key outcome of this research will be to provide direction for future field studies to quantify soil water movement attributes
 396 of New Zealand soils, and to prioritise which measurements will have the greatest value to reduce the uncertainty in
 397 modelling of the soil moisture release and hydraulic conductivity relationships. Recommendations are:

- 398 • Evaluate the spatial representativeness of the current soil physics data set and undertake more measurements of
 399 hydraulic conductivity and soil water retention on key soils.
- 400 • Use larger cores for measurements of hydraulic conductivity.
- 401 • Take measurements of the moisture release curve and saturated hydraulic conductivity on the same sample.
- 402 • Provide more accurate measurements of total porosity.
- 403 • Conduct near saturation measurements of $\theta(h)$ and $K(\theta)$ to better characterize the macropore domain, which is
 404 responsible for preferential flow behaviour.
- 405 • Make more accurate measurements on slowly permeable soils ($< 1 \text{ cm day}^{-1}$), which are important for management
 406 purposes but are not well represented in the current databases.

407 7 Conclusions

408 We report here on further adaptations to the saturated hydraulic conductivity model to suit it to dual-porosity structural soils
 409 (Eq. 10) by computing the soil water flux through a continuous function of an improved Romano et al. (2011) $\theta(h)$ dual
 410 pore-size distribution (Eq. 18). The shape of the improved Romano $\theta(h)$ distribution is identical to the improved $\theta(h)$, but the
 411 advantage of the developed bimodal $\theta(h)$ is that it is more easily parameterized when no data are available in the macropore
 412 domain.

413
 414 The stratification of the data with texture only (loam or clay) slightly improved the predictions of the K_s model, which
 415 is based on pore-size distribution. This gives us confidence that the K_s model is accounting for the effect of these physical
 416 parameters on K_s . A significant improvement was made by separating topsoils from subsoils. The improvements are higher
 417 for the topsoil, which has higher macroporosity caused by roots and tillage compared to subsoils. The reason why a model
 418 with no stratification is not sufficient is unclear and requires further investigation.

419
 420 The improvements made by using the developed bimodal K_{s_bim} (Eq. 18) compared to the unimodal K_{s_uni} (Eq. 8) is
 421 modest overall, but, as expected, greater for topsoils having larger macroporosity. Nevertheless, an acceptable fit between
 422 K_{s_bim} with K_{s_obs} was obtained when due recognition was given to the high variability in the measured data. We expect K_{s_bim}
 423 to provide greater improvement in K_s predictions if more $\theta(h)$ measurements are made at tensions near saturation and if
 424 measurements are made on larger cores and with more accurate measurements of porosity.

425 Data availability

426 The data are part of the New Zealand soil databases, available at <http://smap.landcareresearch.co.nz/> and
 427 <https://soils.landcareresearch.co.nz/>.



428 Acknowledgements

429 We are grateful to Leah Kearns and for Ray Prebble, who improved the readability of the manuscript. This project was
 430 funded by Landcare Research core funding, through the New Zealand Ministry of Business, Innovation and Employment.

431

432 References

- 433 Anderson, J. L., and Bouma, J.: Relationships between saturated hydraulic conductivity and morphometric data of an argillic
 434 horizon1, *Soil Sci. Soc. Am. J.*, 37, 408–413, doi:10.2136/sssaj1973.03615995003700030029x, 1973b.
- 435 Arya, L. M., and Paris, J. F.: A physicoempirical model to predict the soil moisture characteristic from particle-size
 436 distribution and bulk density data, *Soil Science Society of America Journal*, 45, 1023–1030,
 437 doi:10.2136/sssaj1981.03615995004500060004x, 1981.
- 438 Balland, V., and Pollacco, J. A. P.: Modeling soil hydraulic properties for a wide range of soil conditions, *Ecological
 439 Modelling*, 219, 300–316, 2008.
- 440 Borgesen, C. D., Jacobsen, O. H., Hansen, S., and Schaap, M. G.: Soil hydraulic properties near saturation, an improved
 441 conductivity model, *Journal of Hydrology*, 324, 40–50, doi:10.1016/j.jhydrol.2005.09.014, 2006.
- 442 Brooks, R. H., and Corey, A. T.: Hydraulic properties of porous media, *Hydrol. Pap.*, 3, 1964.
- 443 Carrick, S.: The dynamic interplay of mechanisms governing infiltration into structured and layered soil columns, PhD,
 444 Lincoln University, Lincoln, 2009.
- 445 Carrick, S., Almond, P., Buchan, G., and Smith, N.: In situ characterization of hydraulic conductivities of individual soil
 446 profile layers during infiltration over long time periods, *European Journal of Soil Science*, 61, 1056–1069,
 447 doi:10.1111/j.1365-2389.2010.01271.x, 2010.
- 448 Carrick, S., Buchan, G., Almond, P., and Smith, N.: Atypical early-time infiltration into a structured soil near field capacity:
 449 the dynamic interplay between sorptivity, hydrophobicity, and air encapsulation, *Geoderma*, 160(3–4), 579–589,
 450 doi:10.1016/j.geoderma.2010.11.006, 2011.
- 451 Childs, E. C., and Collisgeorge, N.: The permeability of porous materials, *Proc. R. Soc. Lon. Ser-A*, 201, 392–405,
 452 doi:10.1098/rspa.1950.0068, 1950.
- 453 Cichota, R., Vogeler, I., Snow, V. O., and Webb, T. H.: Ensemble pedotransfer functions to derive hydraulic properties for
 454 New Zealand soils, *Soil Research*, 51, 94–111, doi:10.1071/sr12338, 2013.
- 455 Durner, W.: Hydraulic conductivity estimation for soils with heterogeneous pore structure, *Water Resources Research*, 30,
 456 211–223, doi:10.1029/93wr02676, 1994.
- 457 Fatt, I., and Dykstra, H.: Relative permeability studies, *T. Am. I. Min. Met. Eng.*, 192, 249–256, 1951.
- 458 Gradwell, M. W.: Methods for physical analysis of soils. New Zealand Soil Bureau Scientific Report No. 10C, 1972.
- 459 Griffiths, E., Webb, T. H., Watt, J. P. C., and Singleton, P. L.: Development of soil morphological descriptors to improve
 460 field estimation of hydraulic conductivity, *Australian Journal of Soil Research*, 37, 971–982, doi:10.1071/sr98066,
 461 1999.
- 462 Haverkamp, R., Leij, F. J., Fuentes, C., Sciortino, A., and Ross, P. J.: Soil water retention: I. Introduction of a shape index,
 463 *Soil Science Society of America Journal*, 69, 1881–1890, doi:10.2136/sssaj2004.0225, 2005.
- 464 Hayashi, Y., Kosugi, K., and Mizuyama, T.: Soil water retention curves characterization of a natural forested hillslope using
 465 a scaling technique based on a lognormal pore-size distribution, *Soil Science Society of America Journal*, 73, 55–64,
 466 2009.
- 467 Jarvis, N. J., and Messing, I.: Near-saturated hydraulic conductivity in soils of contrasting texture measured by tension
 468 infiltrometers, *Soil Science Society of America Journal*, 59, 27–34, 1995.
- 469 Jarvis, N. J.: A review of non-equilibrium water flow and solute transport in soil macropores: principles, controlling factors
 470 and consequences for water quality, *European Journal of Soil Science*, 58, 523–546,
 471 doi:10.1111/j.1365-2389.2007.00915.x, 2007.
- 472 Koener, R.: *Quantile Regression*, Cambridge University Press, New York, 2005.
- 473 Kosugi, K.: Lognormal distribution model for unsaturated soil hydraulic properties, *Water Resources Research*, 32, 2697–
 474 2703, doi:10.1029/96wr01776, 1996.
- 475 Landcare Research, S-map - New Zealand's national soil layer: <http://smap.landcareresearch.co.nz>, 2015.
- 476 Leij, F. J., Alves, W. J., van Genuchten, M. T., and Williams, J. R.: The UNSODA unsaturated soil hydraulic database, in:
 477 *Proceedings of the International Workshop on Characterization and Measurement of the Hydraulic Properties of
 478 Unsaturated Porous Media*, 1269–1281, 1999.



- 479 Leij, F. J., Haverkamp, R., Fuentes, C., Zatarain, F., and Ross, P. J.: Soil water retention: II. Derivation and application of
 480 shape index, *Soil Science Society of America Journal*, 69, 1891–1901, doi:10.2136/sssaj2004.0226, 2005.
- 481 Lilburne, L. R., Hewitt, A. E., and Webb, T. W.: Soil and informatics science combine to develop S-map: a new generation
 482 soil information system for New Zealand, *Geoderma*, 170, 232–238, doi:10.1016/j.geoderma.2011.11.012, 2012.
- 483 Lilly, A., Nemes, A., Rawls, W. J., and Pachepsky, Y. A.: Probabilistic approach to the identification of input variables to
 484 estimate hydraulic conductivity, *Soil Science Society of America Journal*, 72, 16–24, doi:10.2136/sssaj2006.0391,
 485 2008.
- 486 McKenzie, N., and Jacquier, D.: Improving the field estimation of saturated hydraulic conductivity in soil survey, *Australian*
 487 *Journal of Soil Research*, 35, 803–825, doi:10.1071/s96093, 1997.
- 488 McKenzie, N. J., and Cresswell, H. P.: Field sampling. In: *Soil Physical Measurement and Interpretation for Land*
 489 *Evaluation*, CSIRO, Collingwood, Victoria, 2002
- 490 McLeod, M., Aislabie, J., Ryburn, J., and McGill, A.: Regionalizing potential for microbial bypass flow through New
 491 Zealand soils, *Journal of Environmental Quality*, 37, 1959–1967, doi:10.2134/jeq2007.0572, 2008.
- 492 McNeill, S., Webb, T., and Lilburne, L.: Analysis of soil hydrological properties using S-map data., *Landcare Research*
 493 *report 977*, 2012.
- 494 Messing, I., and Jarvis, N. J.: Temporal variation in the hydraulic conductivity of a tilled clay soil as measured by tension
 495 infiltrometers, *Journal of Soil Science*, 44, 11–24, 1993.
- 496 Patil, N. G., and Rajput, G. S.: Evaluation of water retention functions and computer program "ROSETTA" in predicting soil
 497 water characteristics of seasonally impounded shrink-swell soils, *Journal of Irrigation and Drainage*
 498 *Engineering-ASCE*, 135, 286–294, doi:10.1061/(asce)ir.1943-4774.0000007, 2009.
- 499 Pollacco, J. A. P.: A generally applicable pedotransfer function that estimates field capacity and permanent wilting point
 500 from soil texture and bulk density, *Canadian Journal of Soil Science*, 88, 761–774, 2008.
- 501 Pollacco, J. A. P., Nasta, P., Ugalde, J. M. S., Angulo-Jaramillo, R., Lassabatere, L., Mohanty, B. P., and Romano, N.:
 502 Reduction of feasible parameter space of the inverted soil hydraulic parameters sets for Kosugi model, *Soil Science*,
 503 *SS-S-12-00268*, 2013.
- 504 Romano, N. and Nasta, P.: How effective is bimodal soil hydraulic characterization? Functional evaluations for predictions
 505 of soil water balance, *Eur. J. Soil Sci.*, 67(4), 523–535, doi:10.1111/ejss.12354, 2016.
- 506 Romano, N., Nasta, P., Severino, G. and Hopmans, J. W.: Using Bimodal Lognormal Functions to Describe Soil Hydraulic
 507 Properties, *Soil Sci. Soc. Am. J.*, 75(2), 468–480, doi:10.2136/sssaj2010.0084, 2011.
- 508 Rogowski, A. S.: Watershed physics – model of soil moisture characteristic, *Water Resources Research*, 7, 1575–1582, 1971
 509 doi:10.1029/WR007i006p01575, 1971.
- 510 Rubio, C. M.: Applicability of site-specific pedotransfer functions and ROSETTA model for the estimation of dynamic soil
 511 hydraulic properties under different vegetation covers, *Journal of Soils and Sediments*, 8, 137–145,
 512 doi:10.1065/jss2008.03.281, 2008.
- 513 Schaap, M. G., and van Genuchten, M. T.: A modified Mualem-van Genuchten formulation for improved description of the
 514 hydraulic conductivity near saturation, *Vadose Zone Journal*, 5, 27–34, 2006.
- 515 ter Braak, C. J. F., and Vrugt, J. A.: Differential evolution Markov chain with snooker updater and fewer chains, *Statistics*
 516 *and Computing*, 4, 435–446, 2008.
- 517 van Genuchten, M. T.: Closed-form equation for predicting the hydraulic conductivity of unsaturated soils, *Soil Science*
 518 *Society of America Journal*, 44, 892–898, 1980.
- 519 van Genuchten, M. T., Leij, F. J., and Yates, S. R.: The RETC code for quantifying the hydraulic functions of unsaturated
 520 soils, *The RETC Code for Quantifying the Hydraulic Functions of Unsaturated Soils*, U.S. Department of Agriculture,
 521 *Agricultural Research Service 1991*.
- 522 Vervoort, R. W., and Cattle, S. R.: Linking hydraulic conductivity and tortuosity parameters to pore space geometry and
 523 pore-size distribution, *Journal of Hydrology*, 272, 36–49, 2003.
- 524 Watt, J. P. C., and Griffiths, E.: Correlation of hydraulic conductivity measurements with other physical properties New
 525 Zealand, *New-Zealand Soil Bureau Commentaries*, 1983, 198–201, 1988.
- 526 Webb, T. H., Claydon, J. J., and Harris, S. R.: Quantifying variability of soil physical properties within soil series to address
 527 modern land-use issues on the Canterbury plains, New Zealand, *Australian Journal of Soil Research*, 38, 1115–1129,
 528 doi:10.1071/sr99091, 2000.
- 529 Webb, T. H.: Identification of functional horizons to predict physical properties for soils from alluvium in Canterbury, New
 530 Zealand, *Australian Journal of Soil Research*, 41, 1005–1019, doi:10.1071/sr01077, 2003.
- 531 Wösten, J. H. M., Lilly, A., Nemes, A., and Le Bas, C.: Final report on the EU funded project using existing soil data to
 532 derive hydraulic parameters for simulation models in environmental studies and in land use planning, *DLO Winand*
 533 *Staring Centre, Wageningen, The Netherlands*, 1998.



534 Wösten, J. H. M., Lilly, A., Nemes, A., and Le Bas, C.: Development and use of a database of hydraulic properties of
535 European soils, *Geoderma*, 90, 169–185, 1999.

536 Young, C. D.: Overview of ROSETTA for estimation of soil hydraulic parameters using support vector machines, *Korean*
537 *Journal of Soil Science & Fertilizer*, 42, 18–23, 2009.

538

539 **Tables**

540 **Table 1. Feasible range of the Kosugi parameters and θ_s is θ measured at 5 kPa.**

541

	θ_s ($\text{cm}^3 \text{cm}^{-3}$)	θ_r ($\text{cm}^3 \text{cm}^{-3}$)	$\log_{10} h_m$ (cm)	σ (-)
Min	θ_5	0.0	1.23	0.8
Max	0.60	0.20	5.42	4.0

542

543

544 **Table 2. Description of the tortuosity parameters.**

545

Tortuosity	Description
τ_1	Takes into account the increased path length due to crookedness of the path. When $\tau_1 = 0$ the flow path is perfectly straight down. When τ_1 increases, the flow path is no longer straight but meanders.
τ_2	Theoretically represents the shape of a microscopic capillary tube. The τ_2 parameter is used to estimate restrictions in flow rate due to variations in pore diameter and pore shape. When $\tau_2 = 0$ the shape of the capillary tube is perfectly cylindrical. When τ_2 increases the tube becomes less perfectly cylindrical, which causes lower connectivity.
τ_3	High porosity soils tend to have large <i>effective pores</i> , $\theta_s - \theta_t$, which tend to be more connected than soils with smaller effective pores, which have more dead-ends. When $\tau_3 = 0$ the connectivity is the same between high and low porosity soils. When τ_3 increases the connectivity of the soil increases (Vervoort and Cattle, 2003; Pollacco et al., 2013). Pollacco et al. (2013) found τ_3 to be the least sensitive parameter.

546

547



548 **Table 3. Theoretical constraints of the K_{s_bim} model.**

549

Constraint	Explanation
$\theta_s > \theta_{s_mac} \gg \theta_r$	Self-explanatory.
$0 < \sigma_{mac} \leq 1.5$	To avoid any unnecessary overlap of θ_{bim} with θ_{bim_mat} .
$1 > \tau_1 > \tau_{1_mac} \geq 0$	Flow in the macropore domain (larger pores) is expected to be straighter than in the matrix domain (smaller pores) due to reduced crookedness of the path.
$1 > \tau_2 > \tau_{2_mac} \geq 0$	It is expected that the shape of the ‘microscopic capillary tube’ of the macropore domain (larger pores) is more perfectly cylindrical than in the matrix domain (smaller pores).
$1 > \tau_3 > \tau_{3_mac} \geq 0$	The macropore domain has larger pores, and therefore it is assumed that the pores are better connected than the matrix pores.

550

551

552 **Table 4. Soil series and classification.**

553

Region	Soil series	No. of horizons		New Zealand classification	Soil taxonomy
		Topsoils	Subsoils		
Canterbury regional study	Eyre	6	8	Weathered Orthic Recent	Haplustepts
	Templeton	9	17	Typic Immature Pallic	Haplustepts
	Wakanui	9	17	Mottled Immature Pallic	Humustepts
	Temuka	9	16	Typic Orthic Gley	Endoaquepts
	Lismore	7	5	Pallic Firm Brown	Dystrustepts
	Hatfield	9	18	Typic Immature Pallic	Humustepts
	Pahau	9	18	Mottled Argillic Pallic	Haplustalf
	Waterton	9	15	Argillic Orthic Gley	Endoaqualfs
Canterbury	Waimakariri		2	Weathered Fluvial Recent	Haplustepts
	Lismore		1	Pallic Orthic Brown	Dystrustepts
	Templeton		6	Typic Immature Pallic	Haplustepts
	Wakanui		2	Mottled Immature Pallic	Humustepts
	Temuka		2	Typic Orthic Gley	Endoaquepts
Manawatu	Hautere		3	Acidic Orthic Brown	Dystrudepts
	Levin		4	Pedal Allophanic Brown	Humudepts
	Levin mottled		4	Mottled Allophanic Brown	Humudepts
	Manawatu		1	Weathered Orthic Recent	Haplustepts
	Paraha		3	Mottled Immature Pallic	Haplustepts
	Westmere		2	Typic Mafic Melanic	Humudepts
Marlborough	Brancott		3	Mottled Fragic Pallic	Haplustepts
	Broadridge		3	Mottled-argillic Fragic Pallic	Haplustalf
	Grovetown		3	Typic Orthic Gley	Endoaquepts
	Raupara		1	Typic Fluvial Recent	Ustifluent
	Wairau		1	Typic Fluvial Recent	Ustifluent
	Woodburn		2	Pedal Immature Pallic	Ustochrept
Otago	Dukes		1	Typic Orthic Gley	Endoaquepts
	Linnburn		2	Alkaline Immature Semiarid	Haplocambids
	Matau		4	Typic Orthic Gley	Endoaquepts
	Otokia		1	Mottled Fragic Pallic	Haplustepts
	Pinelheugh		2	Pallic Firm Brown	Eutrudepts
	Ranfurlly		2	Mottled Argillic Semiarid	Haploargids
	Tawhiti		2	Pallic Firm Brown	Eutrudepts
	Tima		2	Typic Laminar Pallic	Haplustepts
	Waenga		2	Typic Argillic Semiarid	Haploargids
	Wingatui		2	Weathered Fluvial Recent	Haplustepts
Southland	Waikiwi		2	Typic Firm Brown	Humudepts
	Waikoikoi		2	Perch-gley Fragic Pallic	Fragiaqualfs

554



555 **Table 5. Different combinations of texture, layer and $RMSE_{\log10}$ reported by using K_{s_bim} and K_{s_uni} models.**

556

Model form	$RMSE_{\log10}$		
	K_{s_uni}	K_{s_bim}	$K_{s_bim} - K_{s_uni}$
Model with combined texture and layer	0.583	0.560	0.023
Model with texture (loam and clay)	0.577	0.543	0.034
Model with topsoil and subsoil layers	0.450	0.430	0.020

558

559

560

561

562



563 **Table 6. Optimal tortuosity parameters of K_{s_uni} and K_{s_bim} .**

564

		N	RMSE _{log10}	T_1	τ_2	τ_3	T_{1_mac}	τ_{2_mac}	τ_{3_mac}	σ_{mac}
K_{s_bim}	Topsoil	51	0.232	5.007	0.969	0.787	4.734	0.511	0.041	0.322
	Subsoil	181	0.471	6.444	0.859	0.408	3.973	0.642	0.729	1.272
K_{s_uni}	Topsoil	51	0.259	5.859	0.967	0.530	-	-	-	-
	Subsoil	181	0.491	6.484	0.854	0.316	-	-	-	-

565

566

567



568 **Table 7. Descriptive statistics of the optimized θ_{mac} ($\theta_s - \theta_{s,\text{mac}}$), θ_s , h_m and σ Kosugi hydraulic parameters. The bar represents the**
569 **average value, SD the standard deviation and N the number of measurement points.**

	N	$\overline{\theta_{\text{mac}}}$	$SD \theta_{\text{mac}}$	$\overline{\theta_s}$	$SD \theta_s$	$\overline{\theta_{s,\text{mac}}}$	$SD \theta_{s,\text{mac}}$	$\overline{\ln h_m}$	$SD \ln h_m$	$\overline{\sigma}$	$SD \sigma$	$\overline{K_s}$	$SD K_s$
		$(\text{cm}^3 \text{ cm}^{-3})$		$(\text{cm}^3 \text{ cm}^{-3})$		$(\text{cm}^3 \text{ cm}^{-3})$		(cm)		$(-)$		(cm h^{-1})	
Topsoil	51	0.038	0.035	0.48	0.04	0.45	0.04	6.43	1.02	3.00	0.61	167.	101.
Subsoil	181	0.030	0.030	0.42	0.05	0.39	0.06	5.39	1.66	2.64	0.86	19.	42.

570



571 **Table 8. Summary of the quantile regression fit of the log-transformed residuals.**

572

Quantile	a_0		a_1	
	Estimate	95% CI	Estimate	95% CI
$\tau = 0.025$	-0.476	$[-\infty, -0.44]$	-0.574	$[-0.62, \infty]$
$\tau = 0.500$	0.041	$[-0.036, 0.080]$	0.041	$[-0.093, 0.053]$
$\tau = 0.975$	0.357	$[0.332, \infty]$	0.627	$[-\infty, 0.711]$

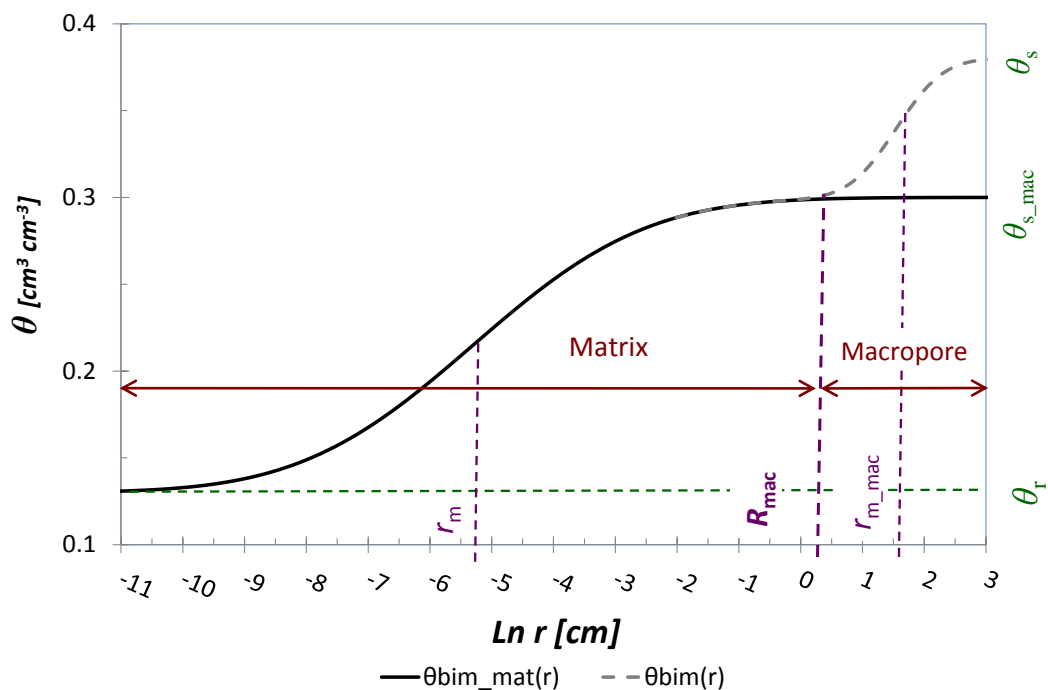
573

574

575



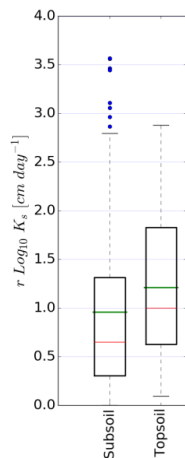
576 **Figures**



577

578 **Figure 1.** A typical Kosugi $\theta_{bim}(r)$ (Eq. (10b)) and $\theta_{bim_mat}(r)$ (Eq. (10c)) with the matrix and macropore domains and the positions
 579 of θ_s , θ_{s_mac} , θ_r , r_m , r_{m_mac} , R_{mac} shown.

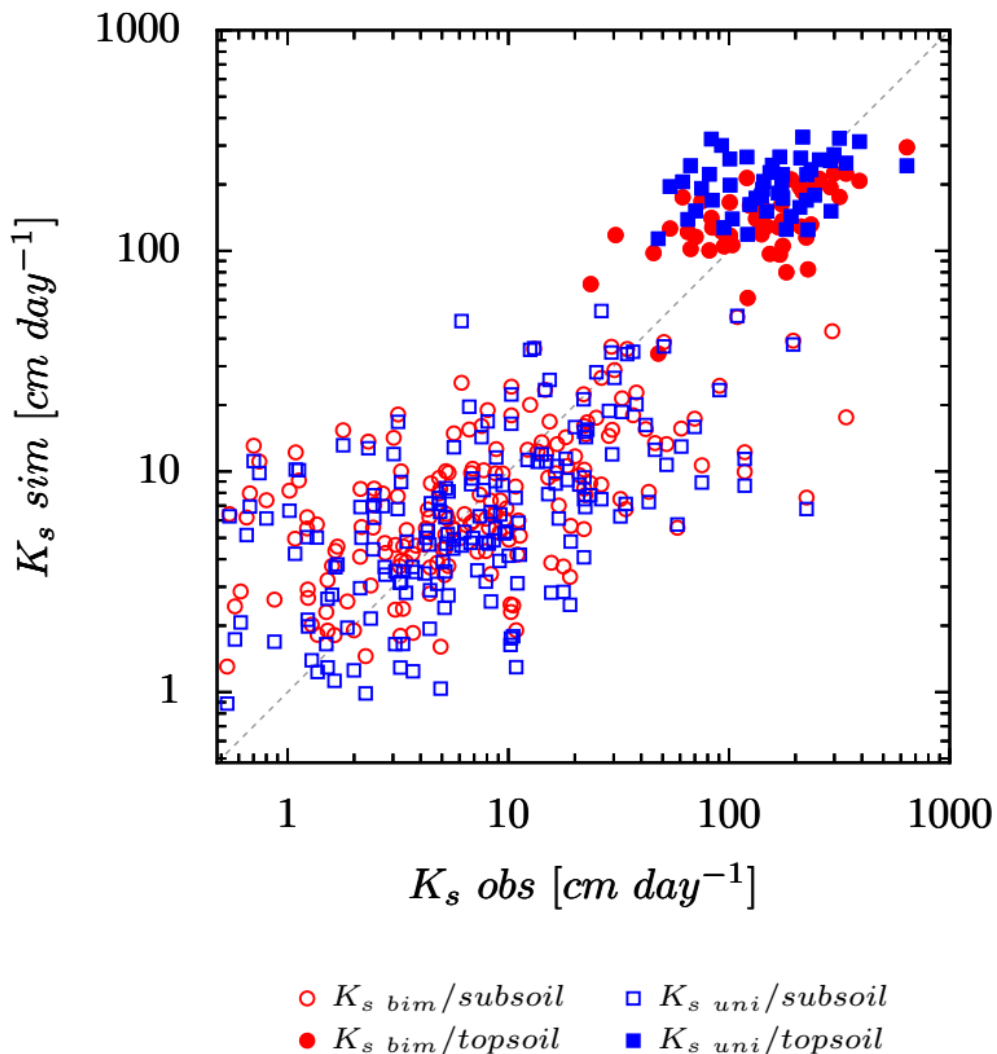
580



581

582 **Figure 2. Uncertainty of the standard error of the observed K_s in topsoil and subsoil. The lines in the box show upper and lower**
583 **quartiles, the median (red), and mean (green). Whiskers show values within 1.5 times the quartile spread; values outside this range**
584 **are shown as plotted points.**

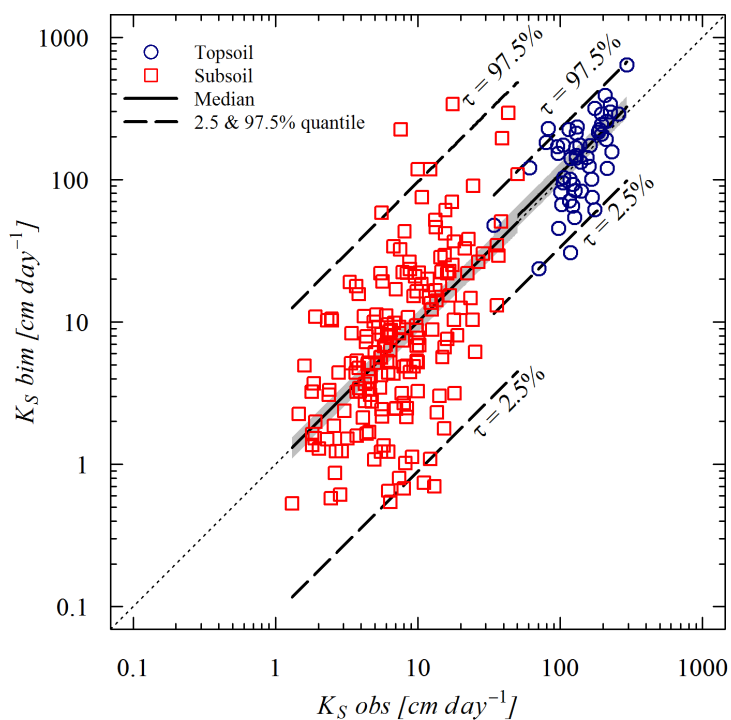
585



586

587 **Figure 3.** Plot between $K_{s,obs}$ against $K_{s,bim}$ and $K_{s,uni}$ for topsoil and subsoil.

588



589
590
591
592

Figure 4. Error of K_{s_bim} plotted against K_{s_obs} for topsoil and subsoil.